

## Research Letter



# Probing charge transfer in 2D MoS<sub>2</sub>/tellurene type-II p-n heterojunctions

Basant Chitara, Department of Chemistry and Biochemistry, North Carolina Central University, Durham, NC 27707, USA Kunyan Zhang, Department of Electrical Engineering, The Pennsylvania State University, University Park, PA 16802, USA Martha Y. Garcia Cervantes, Department of Chemistry and Biochemistry, North Carolina Central University, Durham, NC 27707, USA Tej B. Limbu, Department of Chemistry and Biochemistry, North Carolina Central University, Durham, NC 27707, USA; Department of Physical and Applied Sciences, University of Houston-Clear Lake, Houston, TX 77058, USA

**Bikram Adhikari,** Department of Chemistry and Biochemistry, North Carolina Central University, Durham, NC 27707, USA **Shengxi Huang,** Department of Electrical Engineering, The Pennsylvania State University, University Park, PA 16802, USA **Fei Yan**, Department of Chemistry and Biochemistry, North Carolina Central University, Durham, NC 27707, USA

Address all correspondence to Fei Yan at fyan@nccu.edu

(Received 27 September 2021; accepted 20 October 2021; published online: 3 November 2021)

#### **Abstract**

2D heterostructures offer new opportunities for harnessing a wider range of the solar spectrum in high-performance photovoltaic devices. Here, we explore a type-II p—n heterojunction, by exploiting air-stable tellurene (Te) in combination with  $MoS_2$ , to study its charge transfer for photovoltaic applications. The charge transfer of  $MoS_2$ /Te heterojunction is confirmed by photoluminescence spectroscopy, Raman spectroscopy and Kelvin probe force microscopy. The exciton binding energy for  $MoS_2$ /Te heterojunction is estimated to be around 10 meV, which is much lower than that for monolayer  $MoS_2$ . This strategy can be exploited to develop next-generation intrinsically ultrathin light-harvesting devices.

#### Introduction

Two-dimensional (2D) materials due to their ultrathin nature in addition to the weak interlayer forces offer ease of stacking over each other by simple means. The interlayer coupling between stacked atomically thin 2D layers further extends the potential of 2D materials toward unexplored fascinating new phenomena.[1-5] The weak van der Waals interlayer coupling in 2D van der Waals heterojunctions offers new opportunities such as bandgap opening in graphene, [6] band alignment engineering,<sup>[7]</sup> charge transfer<sup>[8–11]</sup> and enhanced optical absorption.<sup>[12]</sup> In contrary, the realization of these heterostructures in conventional semiconductor requires expensive growth techniques such as molecular beam epitaxy, and metal organic chemical vapor deposition (MOCVD). Although stacking different 2D materials over each other is fundamentally interesting, their creation in commercial applications requires a low-cost technique that can produce a large area of heterostructures. Novel optoelectronic and photovoltaic applications can be realized by stacking different layered materials, such as transition metal dichalcogenides (TMDCs), forming heterostructures. Depending on their layer thickness, their optical bandgaps could cover near-to-mid-infrared spectral range with strong light-matter interactions. To cover the infrared (IR) spectrum for photovoltaic applications, the available low bandgap 2D materials such as black phosphorus (BP) are prone to air degradation. [13]

Recently, hydrothermally synthesized air-stable p-type 2D tellurene (Te) exhibiting a tunable bandgap (0.3–1 eV) has gained a lot of attention due to its intriguing electronic

and optoelectronic properties. The small but tunable bandgap makes Te a promising candidate for IR photodetection. Te exhibits a trigonal crystal lattice where Te atoms are covalently bonded to form helical chains along the c-axis and these spiral chains are combined by weak van der Waals interactions to form a hexagonal lattice structure.<sup>[14]</sup> Te has already been exploited for piezoelectric, [15] thermoelectric, [16] fast photodetecting applications.[17,18] Depending on their layer thickness, their optical bandgap covers near-IR to visible spectral range with strong light-matter interactions. Solution synthesis also offer enormous possibilities of functionalization to tune their electronic and optical properties. Moreover, chemical synthesis of Te offers additional advantage where devices can be easily fabricated via simple solution processing techniques such as drop casting, spin coating, and dip coating. Thus, it would be interesting to explore the true potential of Te by combining it with TMDCs to investigate their charge transfer via creating  $MX_2$ /Te heterojunction for optoelectronic applications.

Heterostructures consisting of graphene and TMDCs have been extensively explored for novel optoelectronic and photovoltaic applications. A key benefit of TMDCs is that they have a much needed optical bandgap spanning near-IR to visible wavelength range and exhibit extremely significant light-matter interactions. [2,19,20] Most of the TMDCs heterostructures form type-II semiconductor heterojunctions that facilitate efficient electron—hole separation for light detection and harvesting. [3] Type-II heterojunctions are formed when both the conduction and valence band edges of one semiconductor are

lower than those corresponding edges of another semiconductor in close proximity. Hence, electrons are confined in one material and the holes in the other material, promoting efficient electron—hole separation and inhibiting their recombination.

## **Experimental** Synthesis of Te nanosheets

Earlier reported hydrothermal synthesis was employed to synthesize Te nanosheets. [17] Briefly, PVP (1.5 g) was dissolved in DI water (16 mL) followed by the addition of Na<sub>2</sub>TeO<sub>3</sub> (46 mg) resulting in a clear solution. To this solution, ammonium hydroxide (1.66 mL) and hydrazine monohydrate (0.83 mL) was added before transferring the final solution to a 25 mL Teflon-lined stainless-steel autoclave. Thereafter, the autoclave was placed in a pre-heated air oven at 180°C for 3 hours. The final product was obtained by rapid cooling of the autoclave under running water and then washed with DI water three times by centrifugation at 5000 rpm for 10 min. It is worth noting that the majority of the final product are Te nanosheets, while the product also contains Te nanowires.

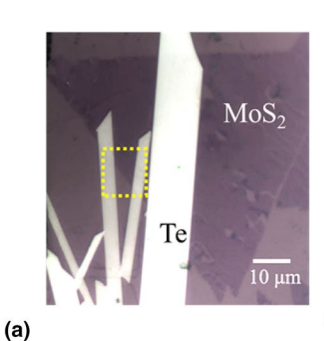
## CVD growth of monolayer MoS<sub>2</sub>

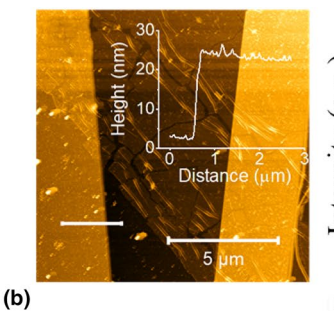
The CVD synthesis of monolayer MoS<sub>2</sub> was performed in CVD (OTF- 1200X, MTI corporation) under ambient pressure conditions. In a typical synthesis, pre-cleaned SiO<sub>2</sub>/Si substrates were placed upside down over an alumina boat containing 5 mg of MoO<sub>3</sub> powder (STREM chemicals Inc.) in a Quartz tube. To this, 200 mg of sulfur powder (Fisher Scientific) was placed upstream in another alumina boat at 10 cm upstream from the MoO<sub>3</sub> containing alumina boat. The monolayer MoS<sub>2</sub> growth was completed via flowing argon gas (40 sccm) and heating the furnace at a ramp rate of 20°C/min. and then maintaining the furnace at 650°C for 20 min. Thereafter, the furnace was allowed to cool to room temperature under ambient conditions.

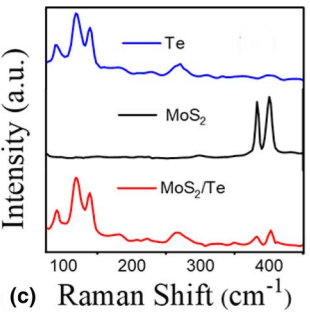
## Fabrication of MoS<sub>2</sub>/Te heterostructure

To realize  $MoS_2/Te$  heterostructure,  $MoS_2$  monolayer was transferred using polydimethylsiloxane (PDMS) stamp on top of the solution-grown Te flakes (drop casted on  $SiO_2/Si$ ) to form  $MoS_2/Te$  heterostructure. To obtain PDMS stamps, 10 parts (by weight, ~20 g) of Sylgard 184 pre-polymer and 1 part (~2 g) of curing agent were mixed in a plastic petri dish.

**Figure 1.** (a) Optical image of MoS<sub>2</sub>/Te heterostructure (b) AFM image of MoS<sub>2</sub>/Te heterostructure taken in the area within the dashed rectangle in a with corresponding height profile of Te shown as inset. (c) Raman spectra of monolayer MoS<sub>2</sub>, Te and MoS<sub>2</sub>/Te heterostructure.







The bubbles resulted after mixing were removed by placing petri dish in a vacuum desiccator for 20 min. The PDMS mixture was then taken in another petri dish to obtain PDMS with desired thickness. Thereafter, the petri dish was kept in a hot air oven pre-heated to 100°C for 35 min. PDMS stamps of size  $(\sim 7 \text{ mm} \times 7 \text{ mm})$  were obtained by cutting the PDMS film using a sharp scalpel. PDMS stamp was then placed over MoS<sub>2</sub>/SiO<sub>2</sub> substrates followed by immersing the substrate in buffered HF for 5 min. The PDMS containing monolayer starts floating due to etching of the underneath SiO<sub>2</sub>. The PDMS stamp containing monolayer MoS2 was then washed several times with DI water to remove BHF. Finally, the PDMS stamp with monolayer MoS2 was gently placed onto Te flakes (drop casted on SiO<sub>2</sub>/Si) followed by heating at 80°C for 15 min. PDMS layer was then gently peeled off leaving behind the monolayer MoS<sub>2</sub>/ Te onto the SiO<sub>2</sub> substrates.

#### Characterization

Te and monolayer MoS<sub>2</sub> and MoS<sub>2</sub>/Te were characterized using optical microscopy, Raman microscopy and KPFM microscopy. For Raman, PL and KPFM measurements, we have utilized a HORIBA LabRAM Evolution RAMAN Microscope-Smart SPM atomic force microscope with 532-nm laser. Low-temperature PL measurements were performed on a home-built optical spectrometer coupled with a 600/mm grating. A 532nm continuous wave laser was employed as the excitation and a 50× objective with an NA of 0.4 and a working distance of 18 mm was used to focus the laser. The laser power during the low-temperature measurement was kept at around 0.2 mW. The sample was mounted onto a Janis ST-500 cryostat and pumped to a pressure of  $10^{-5}$  mbar before cooling down to 77 K by liquid nitrogen. The temperature was controlled by the Lakeshore Model 335 temperature controller. For KPFM measurements, we utilized Si tips with Cr (20 nm)/Au (30 nm) coating and a tip apex radius of < 35 nm purchased from NanoAndMore, USA (product: HQ:NSC14/Cr-Au). The tips were excited to oscillate near their resonance frequency of 160 kHz.

#### **Results and discussion**

Figure 1(a) shows the schematic representation of MoS<sub>2</sub>/Te vertical heterostructure with an optical image of MoS<sub>2</sub>/Te heterostructure used for the Raman and PL characterization.



Figure 1(b) depicts the atomic force microscopy (AFM) image of  $MoS_2$ /Te heterostructure with corresponding height profile with Te shown as inset. The thickness of Te nanosheets is approximatively 20 nm with a lateral dimension around 50  $\mu$ m as evident from the optical image.  $MoS_2$ /Te heterostructure with greater Te thickness is presented in the supplementary information (Fig. S1).

The Raman spectra of MoS<sub>2</sub>, Te and MoS<sub>2</sub>/Te heterostructure are shown in Fig. 1(c). CVD-grown MoS2 exhibits the characteristic Raman vibrations with  $E^1_{2\mathrm{g}} \approx 385~\mathrm{cm}^{-1}$  and  $A_{1\mathrm{g}}$  $\approx 405 \text{ cm}^{-1}$ . The difference of 20 cm<sup>-1</sup> confirms the formation of single layer MoS<sub>2</sub> as reported in literature. [21,22] For Te, the active modes located at  $\sim 91.4 \text{ cm}^{-1}$  ( $E_1 \text{ mode}$ ),  $\sim 119.0 \text{ cm}^{-1}$  $(A_1 \text{ mode})$  and  $\sim 139.2 \text{ cm}^{-1}$   $(E_2 \text{ mode})$  were found, confirming the high quality of Te nanosheets. The Raman spectrum of the MoS<sub>2</sub>/Te heterostructure appears to comprise a combination of all Raman modes from the constituent layers. Interestingly, we observe the quenching of MoS<sub>2</sub> Raman peaks in MoS<sub>2</sub>/ Te heterostructure. The decreased phonon intensity for MoS<sub>2</sub> in the heterostructure can be partially attributed to less photon absorption due to the change of dielectric environment. Natarajan et al.<sup>[23]</sup> also explained the Raman quenching in the n-SnS<sub>2</sub>/p-rGO by a mechanism similar to that for grapheneenhanced Raman scattering, which is related to charge transfer and dipole-dipole coupling. The charge transfer could lead to weaker population of phonon and PL quenching. Similar Raman quenching of MoS<sub>2</sub> over thicker Te flakes with thickness around 75 nm (as shown in Fig. S2).

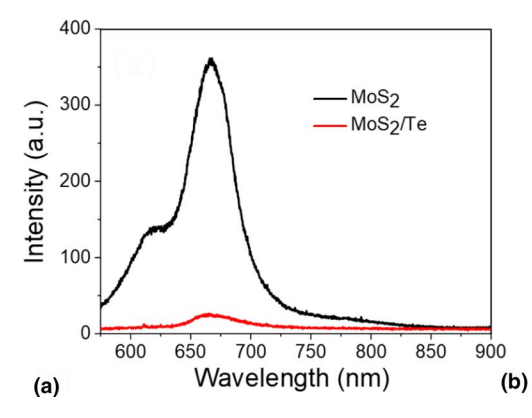
The charge transfer in MoS<sub>2</sub>/Te heterostructure was probed via photoluminescence spectroscopy. The PL spectra for MoS2 and the MoS<sub>2</sub>/Te heterostructure are shown in Fig. 2(a). Figure 2(a) clearly shows two characteristic peaks around 1.85 eV (A) and 1.99 eV (B) for MoS<sub>2</sub> due to the direct bandgap transition from the highest spin–orbital split valence bands at K (K') point to the lowest conduction bands. However, in the case of MoS<sub>2</sub>/Te heterostructure, a strong PL quenching was observed, indicating a charge transfer at the interface of MoS<sub>2</sub>/Te heterostructure. To further verify the local PL behavior of the MoS<sub>2</sub>/Te, a PL intensity map (Fig. 2(b)) at the MoS<sub>2</sub> A-exciton resonance (1.85 eV) was obtained with a 532-nm laser excitation. We chose A-excitonic peak at 1.85 eV rather

than that at 1.99 eV because the former peak has higher intensity. Moreover, the position of A-excitonic peak is independent of the thickness of the  $MoS_2$  owing to the direct gap transition between the maximum of the valence band and the minimum of the conduction band at the K point of the Brillouin zone in monolayer  $MoS_2$ . The PL intensity map shows strong photoluminescence for  $MoS_2$ -only region, whereas photoluminescence is significantly quenched in the  $MoS_2$ /Te heterostructure region confirming the charge transfer. Similar PL quenching of  $MoS_2$  over Te was observed for thicker Te ( $\sim 80$  nm) flakes (Supplementary information Fig. S3). In addition, we did not observe any significant shift in the  $MoS_2$  PL wavelength, further confirming the charge transfer in  $MoS_3$ /Te heterostructure.

To gain insights into the charge transfer in MoS<sub>2</sub>/Te, we performed low-temperature PL measurements over MoS<sub>2</sub>/Te heterostructure from 77 K to room temperature. The typical blue shift was observed for the A-exciton emission peak for MoS<sub>2</sub> in the heterostructure (Fig. 3(a)) with decreasing temperature corresponding to lattice expansion with increasing temperature. The intensity of the A-exciton also decreases as a function of temperature as shown in Fig. S4. To estimate the binding energy of MoS<sub>2</sub>/Te heterostructure, we have utilized the following equation  $I(T) = I_0 / (1 + Ae^{-E}_B / E^T)$  where  $I_0$ is the PL intensity at  $0~{\rm K}, E_{\rm B}$  is the exciton binding energy, and  $k_{\rm B}$  is the Boltzmann constant.<sup>[24]</sup> The binding energy of interlayer exciton for MoS<sub>2</sub>/Te was estimated to be around 10 meV (Fig. 3(b)). The exciton binding for monolayer MoS<sub>2</sub> is about 75 meV,<sup>[24]</sup> which is much higher than that for MoS<sub>2</sub>/Te heterostructure. The lower exciton binding energy for MoS<sub>2</sub>/Te heterostructure indicates that the excitons in the heterostructure can dissociate into free carriers easier than single monolayer MoS<sub>2</sub>. This is an advantage for MoS<sub>2</sub>/Te heterostructure as efficient photodetectors.

We have also employed KPFM to characterize the MoS<sub>2</sub>/Te heterostructure for charge transfer. KPFM techniques via mapping work function provide the information about the composition and electronic states of the local structures of the MoS<sub>2</sub>/Te heterostructure. The surface potential map of MoS<sub>2</sub>/Te heterostructure is shown in Fig. 4. The contact potential difference (CPD) between the AFM tip and Te or MoS<sub>2</sub> can be expressed as CPD<sub>Te</sub>= $\varphi_{tip}\varphi_{Te}$  and CPD<sub>MoS2</sub>= $\varphi_{tip}$ - $\varphi_{MoS2}$  where

**Figure 2.** (a) PL spectra of monolayer MoS<sub>2</sub> and MoS<sub>2</sub>/Te heterostructure, and (b) PL map of MoS<sub>2</sub>/Te heterostructure with corresponding optical image shown as an inset.



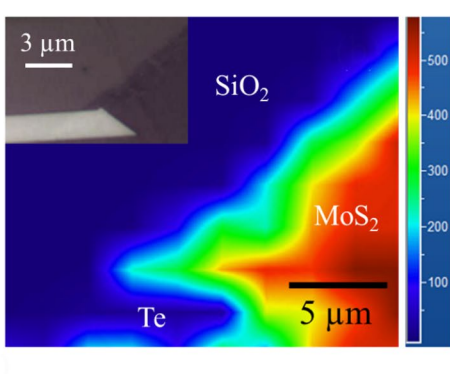


Figure 3. (a) PL peak energy for MoS<sub>2</sub>/Te heterostructure plotted as a function of temperature. (b) The intensity of temperature dependent PL of the MoS<sub>2</sub>/Te heterostructure. The empty circles are the experimental points, and the solid lines are fits to the equations.

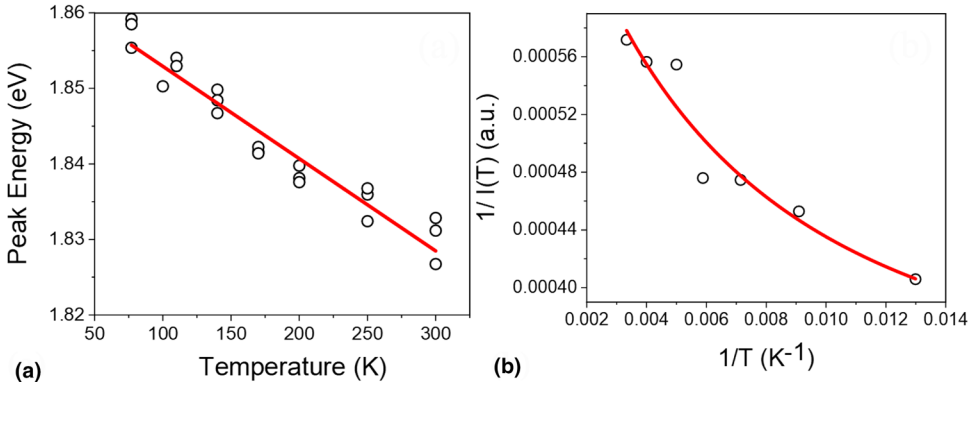
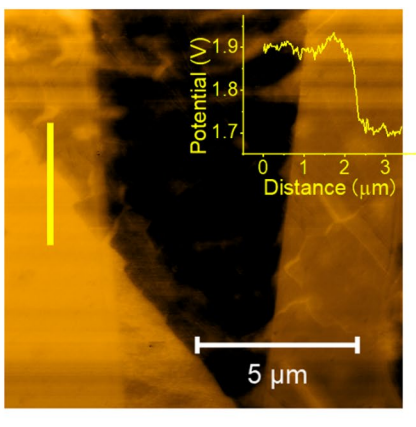
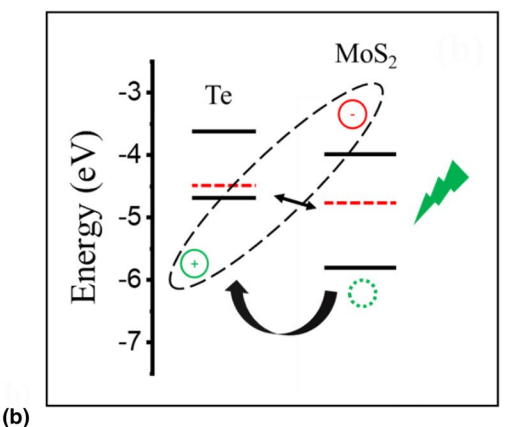


Figure 4. (a) KPFM surface potential map of MoS<sub>2</sub>/Te heterostructure with surface potential profile measured along the yellow solid line (from bottom to top) shown as inset. (b) Band alignment of MoS<sub>2</sub>/Te heterostructure forming a type-II heterojunction.





 $\phi_{\rm tip},\,\phi_{\rm MoS2}$ , and  $\phi_{\rm Te}$  are the work functions of the tip, MoS<sub>2</sub>, and Te, respectively. From the surface potential map, one can clearly see that MoS<sub>2</sub> is lying over Te forming MoS<sub>2</sub>/Te vertical heterostructure. The CPD difference of MoS<sub>2</sub> and Te corresponds to fermi level difference of MoS<sub>2</sub> and Te with difference being the value  $\Delta E_F \sim 250$  meV estimated via line profile of the surface potential as shown in Fig. 4(a). The energy band alignment of the MoS<sub>2</sub>/Te heterostructure<sup>[25,26]</sup> is shown in Fig. 4(b). It is evident from the figure that fermi level of Te is higher than that of MoS<sub>2</sub>. Thus, the vertical MoS<sub>2</sub>/Te heterostructure forms a type-II heterojunction serving a p–n junction. The electrons and holes corresponding to separate regions can be separated due to the built-in potential of the MoS<sub>2</sub>/Te heterojunction causing will lead to efficient charge transfer as supported by PL quenching.

(a)

### Conclusion

In summary, we have experimentally demonstrated, for the first time, the charge transfer in MoS<sub>2</sub>/Te heterostructures. The charge transfer in such heterostructures is probed via PL mapping, low-temperature PL and KPFM measurements. We have estimated the exciton binding energy for MoS<sub>2</sub>/Te p—n heterojunction to be around 10 meV, which is much

lower than that of monolayer MoS<sub>2</sub> (75 meV). The efficient charge transfer manifesting as strong PL quenching in MoS<sub>2</sub>/Te heterostructure makes them potential candidates for tuning the optoelectronic properties of TMDs. This light-harvesting strategy can serve as the next-generation TMD/Te, intrinsically ultrathin p—n junctions-based photovoltaic applications. In addition, the creation of such heterojunctions consisting of Te and other 2D materials further modifies the Schottky barrier heights, which may lead to the suppression of dark current in Te-based photodetectors.

## **Acknowledgments**

The authors are grateful for the financial support of this project by the U.S. National Science Foundation (Awards # 1831133 and #2122044). S.H. acknowledges the support from the National Science Foundation under Grant No. ECCS-1943895. This work was performed in part at the Duke University Shared Materials Instrumentation Facility (SMIF), a member of the North Carolina Research Triangle Nanotechnology Network, which is supported by the National Science Foundation under Grant ECCS-1542015 as part of the National Nanotechnology Coordinated Infrastructure.



#### Author contributions

BC conceived the idea and performed device integration, BC, MC, TL and BA carried out the synthesis and characterization, KZ and SH performed low-temperature PL measurements, BC, KZ and SH analyzed the results. All authors reviewed and revised the manuscript. FY supervised the project.

### **Declarations**

### **Conflict of interest**

Authors have no conflict of interest.

## **Data availability**

The data that support the findings of this study are available from the corresponding author upon reasonable request.

### Supplementary Information

The online version contains supplementary material available at https://doi.org/10.1557/s43579-021-00117-w.

#### References

- A.K. Geim, I.V. Grigorieva, Van der Waals heterostructures. Nature 499, 419-425 (2013)
- L. Britnell, R.M. Ribeiro, A. Eckmann, R. Jalil, B.D. Belle, A. Mishchenko, Y.-J. Kim, R.V. Gorbachev, T. Georgiou, S.V. Morozov, A.N. Grigorenko, A.K. Geim, C. Casiraghi, A.H.C. Neto, K.S. Novoselov, Strong light-matter interactions in heterostructures of atomically thin films. Science 340, 1311-1314 (2013)
- X. Hong, J. Kim, S.-F. Shi, Y. Zhang, C. Jin, Y. Sun, S. Tongay, J. Wu, Y. Zhang, F. Wang, Ultrafast charge transfer in atomically thin MoS<sub>2</sub>/WS<sub>2</sub> heterostructures. Nat. Nanotechnol. 9, 682-686 (2014)
- M.S. Choi, G.-H. Lee, Y.-J. Yu, D.-Y. Lee, S.H. Lee, P. Kim, J. Hone, W.J. Yoo, Controlled charge trapping by molybdenum disulphide and graphene in ultrathin heterostructured memory devices, Nat. Commun. 4, 1624 (2013)
- B. Yan, G. Li, B. Shi, J. Liu, H. Nie, K. Yang, B. Zhang, J. He, 2D tellurene/ black phosphorus heterojunctions based broadband nonlinear saturable absorber. Nanophotonics. 9, 2593-2602 (2020)
- Z. Guan, S. Ni, S. Hu, Band gap opening of graphene by forming a graphene/ PtSe<sub>2</sub> van der Waals heterojunction. RSC Adv. 7, 45393-45399 (2017)
- O. Leenaerts, S. Vercauteren, B. Partoens, Band alignment of lateral twodimensional heterostructures with a transverse dipole. Appl. Phys. Lett. **110**, 181602 (2017)
- A. Du, S. Sanvito, Z. Li, D. Wang, Y. Jiao, T. Liao, Q. Sun, Y.H. Ng, Z. Zhu, R. Amal, S.C. Smith, Hybrid graphene and graphitic carbon nitride nanocomposite: gap opening, electron-hole puddle, interfacial charge transfer, and enhanced visible light response. J. Am. Chem. Soc. 134, 4393-4397
- X. Mu, M. Sun, Interfacial charge transfer exciton enhanced by plasmon in 2D in-plane lateral and van der Waals heterostructures. Appl. Phys. Lett. **117**, 091601 (2020)
- 10. A. Boulesbaa, K. Wang, M. Mahjouri-Samani, M. Tian, A.A. Puretzky, I. Ivanov, C.M. Rouleau, K. Xiao, B.G. Sumpter, D.B. Geohegan, Ultrafast

- charge transfer and hybrid exciton formation in 2D/0D heterostructures. J. Am. Chem. Soc. 138, 14713-14719 (2016)
- 11. J. Xi, J. Byeon, U. Kim, K. Bang, G.R. Han, J.-Y. Kim, J. Yoon, H. Dong, Z. Wu, G. Divitini, K. Xi, J. Park, T. Lee, S.K. Kim, M. Choi, J.W. Lee, Abnormal spatial heterogeneity governing the charge-carrier mechanism in efficient Ruddlesden-Popper perovskite solar cells. Energy Environ. Sci. **14**, 4915–4925 (2021)
- 12. F. Wu, Y. Liu, G. Yu, D. Shen, Y. Wang, E. Kan, Visible-light-absorption in graphitic c<sub>3</sub>n<sub>4</sub> bilayer: enhanced by interlayer coupling. J. Phys. Chem. Lett. 3, 3330-3334 (2012)
- 13. Y. Huang, J. Qiao, K. He, S. Bliznakov, E. Sutter, X. Chen, D. Luo, F. Meng, D. Su, J. Decker, W. Ji, R.S. Ruoff, P. Sutter, Interaction of black phosphorus with oxygen and water. Chem. Mater. 28, 8330-8339 (2016)
- 14. Y. Wang, G. Qiu, R. Wang, S. Huang, Q. Wang, Y. Liu, Y. Du, W.A. Goddard, M.J. Kim, X. Xu, P.D. Ye, W. Wu, Field-effect transistors made from solution-grown two-dimensional tellurene. Nat. Electron. 1, 228–236 (2018)
- 15. T.I. Lee, S. Lee, E. Lee, S. Sohn, Y. Lee, S. Lee, G. Moon, D. Kim, Y.S. Kim, J.M. Myoung, Z.L. Wang, High-power density piezoelectric energy harvesting using radially strained ultrathin trigonal tellurium nanowire assembly. Adv. Mater. 25, 2920-2925 (2013)
- 16. G. Qiu, S. Huang, M. Segovia, P.K. Venuthurumilli, Y. Wang, W. Wu, X. Xu, P.D. Ye, Thermoelectric performance of 2D tellurium with accumulation contacts. Nano Lett. 19, 1955-1962 (2019)
- 17. M. Amani, C. Tan, G. Zhang, C. Zhao, J. Bullock, X. Song, H. Kim, V.R. Shrestha, Y. Gao, K.B. Crozier, M. Scott, A. Javey, Solution-synthesized high-mobility tellurium nanoflakes for short-wave infrared photodetectors. ACS Nano 12, 7253-7263 (2018)
- 18. C. Shen, Y. Liu, J. Wu, C. Xu, D. Cui, Z. Li, Q. Liu, Y. Li, Y. Wang, X. Cao, H. Kumazoe, F. Shimojo, A. Krishnamoorthy, R.K. Kalia, A. Nakano, P.D. Vashishta, M.R. Amer, A.N. Abbas, H. Wang, W. Wu, C. Zhou, Tellurene photodetector with high gain and wide bandwidth. ACS Nano 14, 303-310
- 19. O. Lopez-Sanchez, D. Lembke, M. Kayci, A. Radenovic, A. Kis, Ultrasensitive photodetectors based on monolayer MoS2. Nat. Nanotechnol. 8, 497-501 (2013)
- 20. W.J. Yu, Y. Liu, H. Zhou, A. Yin, Z. Li, Y. Huang, X. Duan, Highly efficient gate-tunable photocurrent generation in vertical heterostructures of layered materials. Nat. Nanotechnol. 8, 952-958 (2013)
- 21. G. Siegel, Y.P.V. Subbaiah, M.C. Prestgard, A. Tiwari, Growth of centimeterscale atomically thin MoS<sub>2</sub> films by pulsed laser deposition, APL Mater. 3, 056103 (2015)
- 22. C.J. Docherty, P. Parkinson, H.J. Joyce, M.-H. Chiu, C.-H. Chen, M.-Y. Lee, L.-J. Li, L.M. Herz, M.B. Johnston, Ultrafast transient terahertz conductivity of monolayer MoS2 and WSe2 grown by chemical vapor deposition. ACS Nano 8, 11147-11153 (2014)
- V. Natarajan, M. Ahmad, J.P. Sharma, A. Sathya, P.K. Sharma, R. Thangaraj, Interfacial charge-transfer for robust Raman guenching in staggered band aligned n-SnS<sub>2</sub>/p-rGO heterostructures, Appl. Surf. Sci. 550, 149356 (2021)
- 24. X. Zhou, N. Zhou, C. Li, H. Song, Q. Zhang, X. Hu, L. Gan, H. Li, J. Lü, J. Luo, J. Xiong, T. Zhai, Vertical heterostructures based on SnSe<sub>2</sub>/MoS<sub>2</sub> for high performance photodetectors, 2D Mater. 4, 025048 (2017)
- 25. J.-J. Tao, J. Jiang, S.-N. Zhao, Y. Zhang, X.-X. Li, X. Fang, P. Wang, W. Hu, Y.H. Lee, H.-L. Lu, D.-W. Zhang, Fabrication of 1D Te/2D ReS2 mixeddimensional van der waals p-n heterojunction for high-performance phototransistor. ACS Nano 15, 3241-3250 (2021)
- Z. Zhang, Q. Qian, B. Li, K.J. Chen, Interface engineering of monolayer MoS<sub>2</sub>/GaN hybrid heterostructure: modified band alignment for photocatalytic water splitting application by nitridation treatment. ACS Appl. Mater. Interfaces. 10, 17419-17426 (2018)